Effect of an Alternative Disulfide Bond on the Structure, Stability, and Folding of Human Lysozyme†

Munehito Arai,‡ Patrice Hamel,§,|| Eiko Kanaya,§,⊥ Koji Inaka,#,▽ Kunio Miki,#,○ Masakazu Kikuchi,§,× and Kunihiro Kuwajima*,‡

Department of Physics, School of Science, University of Tokyo, 7-3-1 Hongo, Bunkyo-ku, Tokyo 113-0033, Japan, Protein Engineering Research Institute, 6-2-3 Furuedai, Suita, Osaka 565-0874, Japan, Research Laboratory of Resources Utilization, Tokyo Institute of Technology, Nagatsuta, Midori-ku, Yokohama 226-0026, Japan, and Department of Chemistry, Graduate School of Science, Kyoto University, Sakyo-ku, Kyoto 606-8502, Japan

Received September 22, 1999; Revised Manuscript Received December 21, 1999

ABSTRACT: Human lysozyme has four disulfide bonds, one of which, Cys65−Cys81, is included in a long loop of the β-domain. A cysteine-scanning mutagenesis in which the position of Cys65 was shifted within a continuous segment from positions 61 to 67, with fixed Cys81, has previously shown that only the mutant W64CC65A, which has a nonnative Cys64−Cys81 disulfide, can be correctly folded and secreted by yeast. Here, using the W64CC65A mutant, we investigated the effects of an alternative disulfide bond on the structure, stability, and folding of human lysozyme using circular dichroism (CD) and fluorescence spectroscopy combined with a stopped-flow technique. Although the mutant is expected to have a different main-chain structure from that of the wild-type protein around the loop region, far- and near-UV CD spectra show that the native state of the mutant has tightly packed side chains and secondary structure similar to that of the wild-type. Guanidine hydrochloride-induced equilibrium unfolding transition of the mutant is reversible, showing high stability and cooperativity of folding. In the kinetic folding reaction, both proteins accumulate a similar burst-phase intermediate having pronounced secondary structure within the dead time of the measurement and fold into the native structure by means of a similar folding mechanism. Both the kinetic refolding and unfolding reactions of the mutant protein are faster than those of the wild-type, but the increase in the unfolding rate is larger than that of the refolding rate. The Gibbs' free-energy diagrams obtained from the kinetic analysis suggest that the structure around the loop region in the β-domain of human lysozyme is formed after the transition state of folding, and thus, the effect of the alternative disulfide bond on the structure, stability, and folding of human lysozyme appears mainly in the native state.

Elucidating the mechanism of how proteins fold is one of the most important issues in biochemistry. The protein-folding mechanism has been thought to be elucidated by detecting and characterizing intermediate species accumulated during the folding process (*1*). So far, various techniques, including stopped-flow circular dichroism (CD)[1] and fluorescence and pulsed-hydrogen exchange NMR experiments, have been applied to monitor the kinetic folding process and to characterize the folding intermediates (*2*−*8*). Furthermore, protein-engineering techniques have been utilized to map out the structure of the intermediates and the transition state of folding at the residue-specific level (*9*−*12*). These studies have shown the accumulation of kinetic-folding intermediates resembling the compact denatured state observed at equilibrium, called a molten globule state, which has a pronounced secondary structure and a compact shape but lacks the tight packing of side chains (*13*−*15*).

Lysozyme is a protein widely used as a model protein system in protein folding studies (*16*−*21*). Its native structure is composed of two domains. One domain, an α-domain,

† This work is supported by Grants-in-Aid for Scientific Research from the Ministry of Education, Culture, and Science of Japan. P.H. was supported by the French Ministry of Foreign Affairs.

* To whom correspondence should be addressed. Phone: +81-3-5841-4128. Fax: +81-3-5841-4512. E-mail: kuwajima@phys.s.u-tokyo.ac.jp.

‡ Department of Physics, University of Tokyo.

§ Protein Engineering Research Institute.

|| Present address: University of California, Los Angeles, Department of Chemistry and Biochemistry, 607 Charles E. Young Drive East, Los Angeles, CA 90095-1569.

⊥ Present address: Biomolecular Engineering Research Institute, 6-2-3 Furuedai, Suita, Osaka, 565-0874, Japan.

Tokyo Institute of Technology.

▽ Present address: Maruwa Food Industry Co., Ltd., 170 Tsutsui-cho, Nara 639-1123, Japan.

○ Department of Chemistry, Kyoto University.

× Present Address: Department of Bioscience and Biotechnology, Faculty of Science and Engineering, Ritsumeikan University, Kusatsu, Shiga 525-8577, Japan.

[1] Abbreviations: CD, circular dichroism; W64CC65A, mutant human lysozyme in which Trp64 and Cys65 are replaced by Cys and Ala, respectively; NMR, nuclear magnetic resonance; GdnHCl, guanidine hydrochloride; UV, ultraviolet; U, the unfolded state; I, the intermediate; N, the native state; ‡, the transition state; ASA(U), solvent-accessible surface area of a residue in the unfolded state; ASA(N), solvent-accessible surface area of a residue in the native state; ΔASA, ASA(U) − ASA(N); ΔASA^{HP}_{tot}, a total value of hydrophobic residues' ΔASA for a protein; C77AC95A, mutant human lysozyme in which both Cys77 and Cys95 are replaced by Ala.

10.1021/bi9921945 CCC: $19.00
Published on Web 03/04/2000

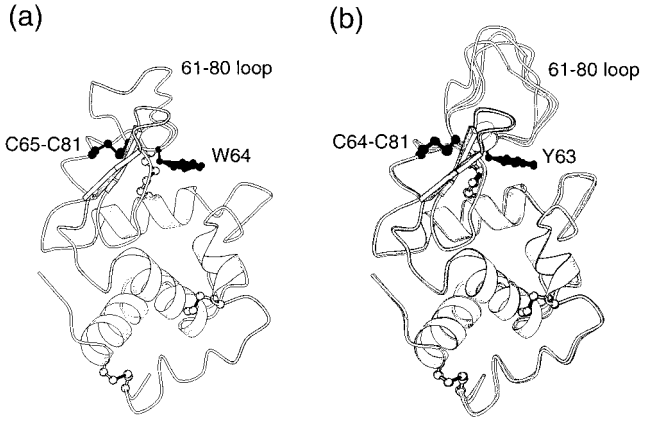

FIGURE 1: Schematic representation of (a) the wild-type (PDB code 1rex) (*24*) and (b) the W64CC65A human lysozymes (PDB code 1qsw) drawn using Molscript (*43*). Four disulfide bonds and Trp64 (a) or Tyr63 (b) are shown by ball-and-stick. (a) Trp64 and the Cys65−Cys81 disulfide bond are shown in black. (b) The structures of four molecules in an asymmetric unit of the crystal are superimposed. Tyr63 and the Cys64−Cys81 disulfide bond are shown in black.

consists of four α-helices (A−D) and one 3_{10}-helix, while the other domain, a β-domain, consists mainly of an antiparallel β-sheet and a long irregular loop (Figure 1). The protein has four disulfide bonds: two of them are involved in the α-domain, one of them is involved in the β-domain (the β-domain disulfide bond), and another links the α-domain to the β-domain (the interdomain disulfide bond). For human lysozyme, the β-domain disulfide bond corresponds to Cys65−Cys81. Kanaya and Kikuchi (*22*) have performed a cysteine-scanning mutagenesis in which the position of Cys65 was shifted within a continuous segment from position 61 to 67, with fixed Cys81, and have found that except the wild-type protein only the mutant W64CC65A, which has a nonnative disulfide bond shifted by one residue, i.e., Cys64−Cys81, can be correctly folded and secreted by yeast. Although the residues 64 and 65 are involved in a long irregular loop spanning from residues 61 to 80, the native structure of the loop region of the wild-type protein has both tight packing of side chains and many hydrogen bonds connected with surrounding regions in the β-domain, and the regions around the β-domain disulfide bond have low *B*-factors in the X-ray crystal structure (*23*−*25*). Therefore, the shift in the position of the β-domain disulfide bond should cause the changes in the main-chain structure and in the side-chain packing around the loop regions. In fact, the crystal structure of the W64CC65A shows that whereas the overall structure of the mutant protein, especially the α-domain, is essentially identical to that of the wild-type protein, the main-chain structure around the 61−80 loop region is highly affected by the Cys64−Cys81 disulfide bond: the cavity created by elimination of Trp64 is filled with Tyr63 in the mutant, and the loop region from positions 67 to 75 is highly flexible (K.I. et al., submitted for publication; see Figure 1). Thus, the W64CC65A mutant is a good model to investigate the effect of an alternative disulfide bond on the structure, stability, and folding of proteins.

Here we studied the structure, stability, and folding mechanism of the wild-type and the W64CC65A mutant human lysozymes by CD and fluorescence spectroscopy. Although the mutant is expected to have the different main-chain and side-chain structures around the loop region from the wild-type, the CD spectra show that it folds into stable native structure with the tightly packed side chains. The analysis of kinetic folding measurements shows that the structure around the 61−80 loop in the β-domain is formed after the transition state of folding and that the effect of the alternative disulfide bond on the structure, stability, and folding of human lysozyme appears only in the native state.

MATERIALS AND METHODS

Materials. Guanidine hydrochloride (GdnHCl) was of specially prepared reagent grade for biochemical use and was acquired from Nakalai Tesque, Inc. (Kyoto, Japan). A concentration of GdnHCl was determined from the refractive index at 589 nm (*26*) with an Atago 3T refractometer. All other chemicals were of guaranteed reagent grade. The W64CC65A mutant human lysozyme was constructed as described (*22*). The wild-type and the mutant human lysozymes were expressed in *Saccharomyces cerevisiae* AH22 and purified as described (*22*, *27*). The proteins were reused after extensive dialysis against water and lyophilization. The reversibility of the unfolding transition and the rate constant of the refolding reaction were checked after every lyophilization. The extinction coefficient of the wild-type and the mutant human lysozymes at 280 nm was 37 700 and 31 940 M^{-1} cm^{-1}, respectively. The latter was calculated by the method of Pace et al. (*28*).

Equilibrium CD Measurements. Equilibrium CD measurements were carried out in a Jasco J-720 spectropolarimeter. Cuvettes with 2 mm and 1 cm path lengths were used for far- and near-UV CD measurements, respectively. Temperature of the cuvettes for all equilibrium and kinetic measurements was controlled at 20.0 ± 0.1 °C by circulating water. Protein concentrations were 2−13 μM throughout the present measurements. All buffers contained 20 mM sodium acetate (pH 5.2). These experimental conditions are identical to those used in Hooke et al. (*19*).

Equilibrium unfolding transitions were analyzed assuming a two-state transition:

$$\theta_{obs} = \frac{(\theta_1 c + \theta_2) + (\theta_3 c + \theta_4)\exp\{(-\Delta G_{NU}{}^0 + m_{NU}{}^{eq} c)/RT\}}{1 + \exp\{(-\Delta G_{NU}{}^0 + m_{NU}{}^{eq} c)/RT\}} \quad (1)$$

where θ_{obs} is the observed ellipticity; θ_1 and θ_3 are the slope of baselines for the native and the unfolded states, respectively; θ_2 and θ_4 are the *y*-intercept of the baselines for the native and the unfolded states, respectively; $\Delta G_{NU}{}^0$ and $m_{NU}{}^{eq}$ are the Gibbs' free energy difference between the native and the unfolded states in water and the cooperativity index of the equilibrium unfolding transition, respectively; *c* is a GdnHCl concentration; and *R* and *T* are gas constant and absolute temperature, respectively (*26*).

Kinetic Measurements. Kinetic CD measurements were carried out in a Jasco J-720 spectropolarimeter. The stopped-flow apparatus attached to the spectropolarimeter was the same as previously described (*3*, *8*, *29*). The mixing ratio was 1:10.0−10.6, the path-length of a cuvette was 3.8 mm, and the dead time was 25 ms. Kinetic fluorescence measurements were performed in a stopped-flow spectrofluorometer

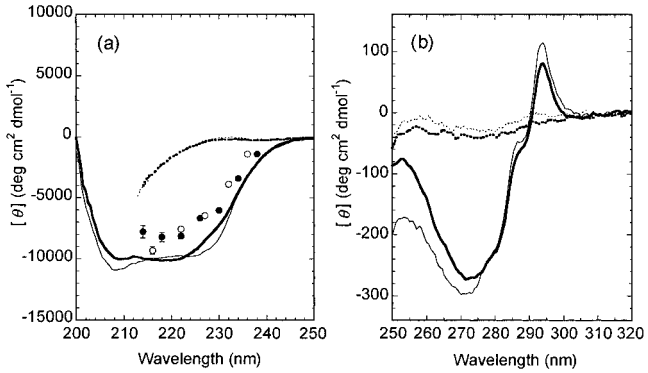

FIGURE 2: (a) Far- and (b) near-UV CD spectra of wild-type (thin lines) and W64CC65A (thick lines) human lysozymes in the native state (solid lines) and the unfolded state at 7 M GdnHCl (dotted lines). Far-UV CD spectra of the burst-phase intermediate of wild-type (open circles) and W64CC65A (filled circles) human lysozymes are also shown in panel a.

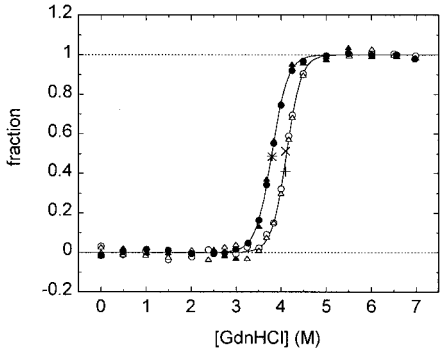

FIGURE 3: GdnHCl-induced equilibrium unfolding transition curves of wild-type (open symbols) and W64CC65A (filled symbols) human lysozymes. The transitions are monitored by far-UV CD at 222 nm (circles) and by near-UV CD at 270 and 274 nm for the wild-type and the W64CC65A mutant, respectively (triangles). Solid lines are theoretical transition curves assuming a two-state transition (eq 1). Cross and plus symbols show the far- and near-UV CD values, respectively, after the protein dissolved in 7 M GdnHCl solution is refolded to the indicated GdnHCl concentration.

specially designed and constructed by Unisoku Inc. (*8*). The excitation wavelength was 280 nm (spectral bandwidth 8 nm) and the emission light at wavelength less than 320 nm was cut off through a cutoff filter. The mixing ratio was 1:9, the path length of a cuvette was 2 mm, and the dead time was 7.5 ms. Refolding reactions were initiated by a concentration jump of GdnHCl from 6.3 and 7.0 M for the stopped-flow fluorescence and CD experiments, respectively. Since the refolding rate was relatively fast and the ellipticity change upon refolding was small, causing a low signal-to-noise ratio of the CD data, the refolding was difficult to be measured by the stopped-flow CD technique. Therefore, the refolding reactions at various GdnHCl concentrations are measured mainly by the stopped-flow fluorescence technique. Unfolding reactions were initiated by a concentration jump of GdnHCl from 0 M and were measured by stopped-flow CD.

Kinetic data were fitted by the nonlinear least-squares method to the following equation:

$$A(t) = A(\infty) + \sum_i \Delta A_i \exp(-k_i t) \qquad (2)$$

where $A(t)$ and $A(\infty)$ are the observed values of the ellipticity or fluorescence at time t and infinite time, respectively, and k_i and ΔA_i are the apparent first-order rate constant and the amplitude of the ith phase, respectively. Because of the low signal-to-noise ratio, refolding curves monitored by CD were analyzed by fixing the refolding rate constants to those obtained from stopped-flow fluorescence experiments under the same conditions.

RESULTS

Far and Near-UV CD Spectra. Figure 2 shows far- and near-UV CD spectra of the wild-type and the W64CC65A mutant human lysozymes in the native and unfolded states. These spectra indicate that the mutant protein has as much secondary and tertiary structure as the wild-type protein in the native state and that both proteins completely lose secondary and tertiary structure in the unfolded state. However, some differences between the spectra of both proteins are present in the native state. In the far-UV region, the peak wavelengths are 208 and 225 nm in the spectrum of the wild-type protein, while those of the mutant protein are 209 and 218 nm (Figure 2a). Since the W64CC65A's crystal structure is essentially identical to that of the wild-type protein, especially in the α-domain (K.I. et al., submitted for publication; Figure 1), this spectral change should be due to the mutations on the tryptophan residue and/or the disulfide bond in W64CC65A, because a tryptophan indole and a disulfide bond are known to generate CD signals even in the far-UV region (*31*, *32*).

In the near-UV region, a decrease in CD intensity is observed at 270 and 293 nm for the mutant lysozyme (Figure 2b). Since optical activity of tryptophans appears in these regions (*32*, *33*), this decrease in CD intensity can be ascribed to the decrease in the number of tryptophan residues in the mutant W64CC65A. A difference in the CD intensities at 250−260 nm is also observed between the mutant and the wild-type proteins. At least two factors may affect the CD intensity in these regions. First, the difference might be caused by the change in the location of a disulfide bond between the wild-type and mutant proteins, because the optical activity of disulfide bonds is known to appear in these wavelength regions (*32*). Second, in the β-domain of human lysozyme there are five aromatic residues, Tyr45, Tyr54, Phe57, Tyr63, and Trp64, two of which are involved in the 61−80 loop. Since the change in the location of the β-domain disulfide bond by the mutations should affect the side-chain packing around the loop region, such rearrangement of packing around the aromatic residues might also contribute to the change in the near-UV CD spectrum at 250−260 nm.

Equilibrium Unfolding Transition. Figure 3 shows GdnHCl-induced unfolding transition curves of the wild-type and the W64CC65A lysozymes. For both proteins, the unfolding transitions are highly cooperative, and the transition curves monitored by far- and near-UV CD are coincident with each other, indicating the absence of equilibrium unfolding intermediates. Therefore, the transition curves are fitted to the theoretical curves of a two-state transition between the native and the unfolded states (see Materials and Methods), and the thermodynamic parameters thus obtained are listed in Table 1. The transition midpoint of the mutant protein is 0.3 M less than that of the wild-type protein, and the Gibbs' free-energy difference between the native and the unfolded states at 0 M GdnHCl, ΔG_{NU}^0, is similar for both proteins

Table 1: Thermodynamic Parameters of GdnHCl-Induced Equilibrium Unfolding Transitions

proteins	c_M (M)	m_{NU}^{eq} (kcal/mol M)	ΔG_{NU}^0 (kcal/mol)
wild-type	4.12 ± 0.01	3.6 ± 0.1	14.7 ± 0.5
W64CC65A	3.79 ± 0.01	3.30 ± 0.09	12.5 ± 0.4

[a] c_M, m_{NU}^{eq}, and ΔG_{NU}^0 are the midpoint GdnHCl concentration, the cooperativity index of the transition, and the Gibbs' free-energy difference between the native and the unfolded states in water, respectively. Errors are standard deviations of fitting.

(Table 1). These results indicate that the mutant protein forms a stably folded structure in the native state.

A cooperativity index, m_{NU}^{eq}, is known to be proportional to a difference in the solvent-accessible surface area of hydrophobic residues between the native and the unfolded states (*34*, *35*). The m_{NU}^{eq} value of the mutant protein is close to that of the wild-type protein, indicating that most of the hydrophobic residues of the mutant are buried inside the molecule. A difference of the m_{NU}^{eq} value between the wild-type and the mutant may be due to the structural changes around the Cys64−Cys81 disulfide bond in the mutant (see Discussion).

To investigate the reversibility of the unfolding transition, each protein was first dissolved in 7 M GdnHCl solution and an attempt was subsequently made to refold it by a concentration jump of GdnHCl to the concentration of the transition midpoint. The results show that for both the wild-type and the mutant proteins, the CD intensity after the refolding is coincident with that obtained by the equilibrium unfolding measurement (Figure 3), demonstrating that the unfolding transitions of both proteins are fully reversible.

Kinetic Refolding and Unfolding Reactions. Kinetic refolding and unfolding reactions of the mutant and wild-type proteins with intact disulfide bonds were measured using stopped-flow fluorescence and CD techniques. Figure 4 shows the representative refolding and unfolding curves. In the refolding of both proteins, two phases—a fast phase and a slow phase—were observed. The amplitude of the slow phase is about 20% and 10% of the total amplitude of the two phases for the wild-type and mutant proteins, respectively, showing that the slow phase is the minor phase. The GdnHCl dependence of the logarithm of the refolding/unfolding rate constant, called a "chevron plot", is shown in Figure 5. The rate constant of the fast phase in the refolding of W64CC65A is slightly larger than that of the wild-type at 0−2.5 M GdnHCl, showing that the presence of the alternative disulfide bond does not interfere with the refolding process of human lysozyme. Although the refolding rate of the mutant is slightly larger than that of the wild-type, the increase in the unfolding rate of the mutant protein is more significant than that in the refolding rate (Figures 4 and 5).

Figure 5 also shows that the chevron plot for the fast phase bends over at low GdnHCl concentrations. This behavior is referred to as a "rollover" and is indicative of the accumulation of a folding intermediate(s) within the dead time of the stopped-flow measurement, i.e., within the burst phase (*36*). The accumulation of an intermediate is also suggested by burst signal change in CD. When the refolding reaction is monitored by the stopped-flow CD technique at a low GdnHCl concentration and at 222 nm, about 70% of the full

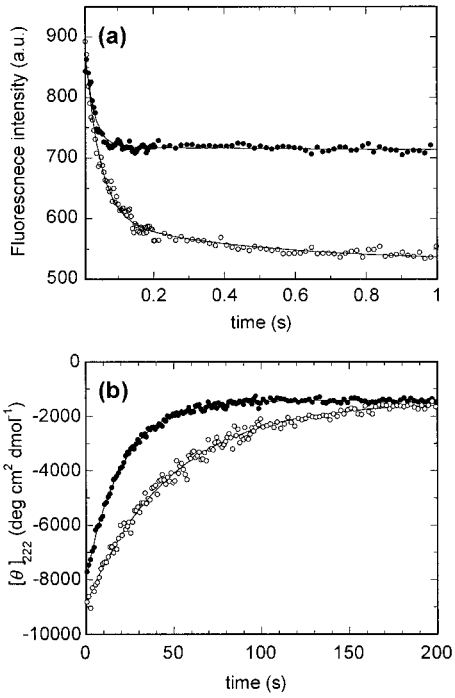

FIGURE 4: Kinetic refolding (a) and unfolding curves (b) of wild-type (open circles) and W64CC65A (filled circles) human lysozymes. Solid lines are fitting curves (eq 2). (a) The refolding was initiated by a GdnHCl concentration jump from 6.3 to 0.6 M and monitored by tryptophan fluorescence. (b) The unfolding reaction was initiated by a GdnHCl concentration jump from 0 to 6 M and monitored by CD at 222 nm.

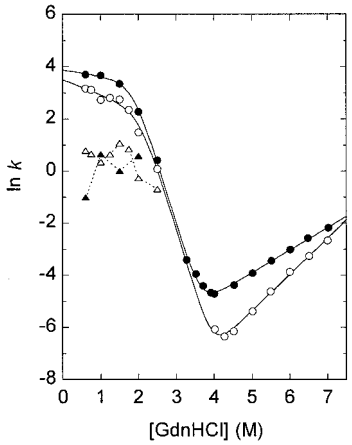

FIGURE 5: GdnHCl dependence of refolding and unfolding rate constants (chevron plot) of wild-type (open symbols) and W64CC65A (filled symbols) human lysozymes. Rate constants at more than 3 M GdnHCl are obtained by unfolding measurements using stopped-flow CD. The rate constants of the fast and slow phases of the refolding reaction (<3 M GdnHCl) measured by stopped-flow fluorescence are shown by circles and triangles, respectively. Solid lines are theoretical curves fitted to eq 3.

ellipticity change expected between the unfolded and the native states was regained within the burst phase (Figure 2a). Thus, these results clearly show the accumulation of a burst-phase intermediate having a pronounced secondary structure under strongly native conditions.

Figure 4a shows that the fluorescence intensities of the burst-phase intermediate obtained by extrapolating the refolding curves to zero time are similar for the wild-type and the mutant proteins, indicating that similar structures are formed for the intermediates of both proteins. Our prelimi-

nary data show that there is a burst phase in the refolding reactions of both proteins monitored by fluorescence (data not shown). This indicates that hydrophobic residues, especially tryptophan residues, are buried inside a protein molecule in the intermediate. On the other hand, the fluorescence intensity after the refolding, i.e., in the native state, is smaller for the wild-type protein, which might be caused by fluorescence quenching in the presence of Trp64 in the wild-type.

The structure of the burst-phase intermediate is further investigated by measuring the refolding reaction of the wild-type and mutant proteins by stopped-flow CD at different wavelengths. Since the burst phase is kinetically uncoupled to the subsequent folding phases, the equilibrium between the unfolded state and the burst-phase intermediate can be rapidly reached within the burst phase. Thus, the amplitude of the burst phase is directly related to the population of the intermediate, and the ellipticity values extrapolated to zero time of the refolding curves measured at different wavelengths construct the CD spectrum of the burst-phase intermediate (Figure 2a). The results show that the CD spectra of the burst-phase intermediate of the wild-type and the W64CC65A mutant are close to each other, indicating that the secondary structure of the burst-phase intermediate of the mutant protein is similar to that of the wild-type protein.

Kinetic Analysis of the Refolding and Unfolding Reactions. To obtain the thermodynamic parameters of the refolding and unfolding reactions, the kinetics of these reactions were analyzed with a three-state model involving the unfolded (U), the intermediate (I), and the native states (N). In the present analysis, only the faster, major phase is taken into account, because the amplitude of the slower, minor phase is small and because it has been suggested that the slower phase is caused by the isomerization of the Cys77−Cys95 disulfide bond (*18*). Since the fast track of folding (U → N) was not observed in pulsed-hydrogen exchange NMR experiments (*19*), we do not consider both the triangle mechanism in which the three states are mutually connected (*37*) and the off-pathway model in which the intermediate is a dead-end product (I ⇄ U ⇄ N). Therefore, the sequential three-state model in which the burst-phase intermediate is an on-pathway intermediate is used for the analysis of the folding reaction of human lysozyme:

$$\mathrm{U} \underset{k_{\mathrm{IU}}}{\overset{k_{\mathrm{UI}}}{\rightleftharpoons}} \mathrm{I} \underset{k_{\mathrm{NI}}}{\overset{k_{\mathrm{IN}}}{\rightleftharpoons}} \mathrm{N}$$

where k_{ij} is a microscopic rate constant of a reaction from i to j state (i,j = U, I, or N). Because the formation of the intermediate is considerably faster than the subsequent folding process, the rapid preequilibrium between the intermediate and the unfolded state is assumed. Then the apparent rate constant, k_{app}, is given by

$$k_{\mathrm{app}} = {k_{\mathrm{NI}}}^{0} \exp(m_{\mathrm{N}\ddagger} c/RT) + \frac{{k_{\mathrm{IN}}}^{0} \exp(-m_{\mathrm{I}\ddagger} c/RT)}{1 + 1/\{{K_{\mathrm{UI}}}^{0} \exp(-m_{\mathrm{IU}} c/RT)\}} \quad (3)$$

where $m_{\mathrm{N}\ddagger}/RT$ and $m_{\mathrm{I}\ddagger}/RT$, respectively, are the derivatives of the natural logarithm of the unfolding and refolding rate constants, k_{NI} and k_{IN}, with respect to GdnHCl concentration, c; ${k_{\mathrm{NI}}}^{0}$ and ${k_{\mathrm{IN}}}^{0}$ are the values at zero concentration of GdnHCl; ${K_{\mathrm{UI}}}^{0}$ is an equilibrium constant between the U and the I states at 0 M GdnHCl ($K_{\mathrm{UI}} = [\mathrm{I}]/[\mathrm{U}] = k_{\mathrm{UI}}/k_{\mathrm{IU}}$); and m_{IU}/RT is the derivative of the natural logarithm of K_{UI} (*38*). To simplify the fitting, we assumed that $m_{\mathrm{NU}}^{\mathrm{eq}} = m_{\mathrm{N}\ddagger} + m_{\mathrm{I}\ddagger} + m_{\mathrm{IU}}$ and ${k_{\mathrm{NI}}}^{0}$ and $m_{\mathrm{N}\ddagger}$ values were fixed to the values obtained by fitting the chevron plot linearly at higher GdnHCl concentrations. The chevron plot for the faster, major phase is fitted to eq 3 (see Figure 5), and the parameters thus obtained are given in Table 2. Here, $\Delta {G_{ij}}^{0}$ is the free-energy difference between i and j states in water (i,j = U, I, N, or the transition state, ‡). $\Delta {G_{\mathrm{NU}}}^{0}$(kin) obtained by the kinetic analysis is coincident with that obtained by the equilibrium measurement (Table 2), indicating that ignoring the slower, minor phase does not significantly affect the analysis.

Table 2: Kinetic and Thermodynamic Parameters for the Refolding and Unfolding Reactions of the Wild-Type and the Mutant Human Lysozyme

parameters[a]	wild-type	W64CC65A
${K_{\mathrm{UI}}}^{0}$	$(6 \pm 1) \times 10^{3}$	$(4.9 \pm 0.7) \times 10^{3}$
${k_{\mathrm{NI}}}^{0}$	$(4.4 \pm 0.8) \times 10^{-6}$	$(2.6 \pm 0.3) \times 10^{-4}$
${k_{\mathrm{IN}}}^{0}$	$(3.3 \pm 0.6) \times 10^{1}$	$(4.9 \pm 0.7) \times 10^{1}$
$\Delta {G_{\mathrm{IU}}}^{0}$ [b]	5.0 ± 0.1	4.95 ± 0.09
$\Delta {G_{\mathrm{N}\ddagger}}^{0}$ [b]	24.3 ± 0.2	21.9 ± 0.1
$\Delta {G_{\mathrm{I}\ddagger}}^{0}$ [b]	15.0 ± 0.2	14.9 ± 0.1
$\Delta {G_{\mathrm{NI}}}^{0}$ [b]	9.2 ± 0.2	7.1 ± 0.1
$\Delta {G_{\mathrm{NU}}}^{0}$(kin)[b]	14.2 ± 0.2	12.1 ± 0.2
$\Delta {G_{\mathrm{NU}}}^{0}$ [c]	14.7 ± 0.5	12.5 ± 0.4
m_{IU}	2.5 ± 0.1	2.7 ± 0.1
$m_{\mathrm{I}\ddagger}$	0.33 ± 0.09	0.14 ± 0.08
$m_{\mathrm{N}\ddagger}$	0.81 ± 0.02	0.51 ± 0.01
$m_{\mathrm{NU}}^{\mathrm{eq}}$ [c]	3.6 ± 0.1	3.30 ± 0.09

[a] k, ΔG, and m are in seconds^{-1}, kilocalories per mole, and kilocalories per mole molarity, respectively. [b] Following equations are used: $\Delta {G_{\mathrm{IU}}}^{0} = RT \ln {K_{\mathrm{UI}}}^{0}$, $\Delta {G_{\mathrm{NI}}}^{0} = RT \ln({k_{\mathrm{IN}}}^{0}/{k_{\mathrm{NI}}}^{0})$, $\Delta {G_{\mathrm{NU}}}^{0}(\mathrm{kin}) = \Delta {G_{\mathrm{IU}}}^{0} + \Delta {G_{\mathrm{NI}}}^{0}$, $\Delta {G_{\mathrm{N}\ddagger}}^{0} = RT \ln(k_{\mathrm{B}}T/h) - RT \ln {k_{\mathrm{NI}}}^{0}$, and $\Delta {G_{\mathrm{I}\ddagger}}^{0} = RT \ln(k_{\mathrm{B}}T/h) - RT \ln {k_{\mathrm{IN}}}^{0}$, where k_{B} and h are the Boltzmann constant and the Planck constant, respectively. [c] From Table 1.

DISCUSSION

We studied the structure and stability of the wild-type and the W64CC65A mutant human lysozymes using CD spectroscopy and studied their folding kinetics using the stopped-flow CD and fluorescence techniques. Here we discuss the structure and stability of W64CC65A, the structure around the mutation sites in the intermediate and the transition state of folding, and finally the folding mechanism of human lysozyme.

Structure of the W64CC65A. Comparison of the X-ray crystal structures of the wild-type and the mutant W64CC65A human lysozymes shows that both structures are essentially identical to each other, especially in the α-domain (K.I. et al., submitted for publication; Figure 1). In the present studies, the results of the CD spectra indicate that there should be a difference in side-chain packing around the mutation sites between these two proteins. This is also inferred from a small decrease in the $m_{\mathrm{NU}}^{\mathrm{eq}}$ value of the mutant (Table 1), since the $m_{\mathrm{NU}}^{\mathrm{eq}}$ value is proportional to the difference in the solvent-accessible surface area (ΔASA) of hydrophobic residues between the unfolded and the native states [ASA(U) − ASA(N)] (*34*, *35*).

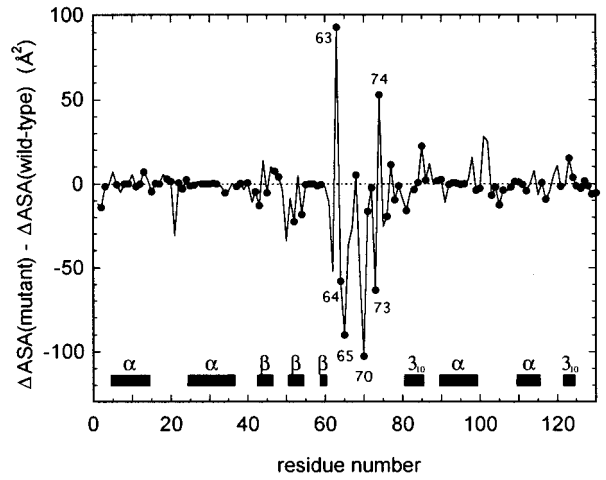

FIGURE 6: The difference in the ΔASA of each residue between the wild-type and the W64CC65A mutant human lysozymes [ΔASA(mutant) − ΔASA(wild-type)]. Positive values indicate that the residue is more buried in the native state of the mutant protein than in the wild-type protein, while the negative values indicate that the residue is more exposed in the native state of the mutant than in the wild-type. Filled circles show the values for hydrophobic residues which have transfer free energy values larger than Ala (*44*). The residue numbers of some residues having large absolute values are shown in the figure. Horizontal bars at the bottom of the figure indicate positions of the secondary structure in the wild-type protein.

To examine which part of the protein molecule is responsible for the difference in the m_{NU}^{eq} value between the wild-type and the mutant lysozymes, we calculated the ΔASA of each residue in these two proteins (Figure 6). For the calculation of ASA(N) by the method of Richmond (*39*), coordinates of the crystal structure of the wild-type (*24*) and the W64CC65A mutant (K.I. et al., submitted for publication) are used. On the other hand, the ASA(U) values were taken from Table 3 of Oobatake and Ooi (*40*), which shows accessible surface areas of atoms of amino acid residues averaged over 132 proteins for random conformation (*41*), so that total value of ASA(U) for the mutant protein is different from that for the wild-type. The results of the calculations show that the ΔASA values of the residues in the α-domain are similar between the two proteins, while the difference in the ΔASA values between them is localized in the loop region from residue 61 to 80 (Figure 6). The results also show that the total value of the hydrophobic residues' ΔASA (ΔASA_{tot}^{HP}) for the mutant is smaller than that for the wild-type protein, and that this difference in the ΔASA_{tot}^{HP} between the two proteins corresponds to 3.5% of the ΔASA_{tot}^{HP} for the wild-type protein. Assuming the proportionality of m_{NU}^{eq} to ΔASA_{tot}^{HP} (*34*, *35*), the mutations in the loop region are thus expected to reduce the m_{NU}^{eq} value of the mutant protein 3.5% less than that of the wild-type, which seems to be in agreement with the experimental results within the experimental error. Therefore, the structural change around the loop region from residue 61 to 80 is responsible for the difference in the m_{NU}^{eq} between the wild-type and the mutant proteins.

The above calculations of the accessible surface areas also show that an increase in the ASA(N) of the residues 61−80 by mutations contributes two-thirds of the difference in the ΔASA_{tot}^{HP} between the wild-type and the mutant, while a decrease in ASA(U) due to the elimination of Trp64 and Cys65 contributes one-third of the difference in the ΔASA_{tot}^{HP}. Therefore, the decrease in the m_{NU}^{eq} of 0.2 kcal/mol M arises from the changes in the native state by mutations, while that of 0.1 kcal/mol M arises from the changes in the unfolded state. It should be noted, however, that the difference in the m_{NU}^{eq} between the wild-type and the mutant proteins is small, indicating that most of the hydrophobic residues of the mutant protein are buried and well-packed in the native state.

Stability of the W64CC65A. The present results show that the ΔG_{NU}^{0} of the W64CC65A mutant is 12.5 (±0.4) kcal/mol, which is 2.2 (±0.6) kcal/mol less than that of the wild-type protein. To understand what causes the difference in the ΔG_{NU}^{0} between the mutant and the wild-type proteins, we calculated the ΔG_{NU}^{0} for each residue of these two proteins using the method of Oobatake and Ooi (*41*) employing the coordinates of the crystal structures of the proteins. Here, ASA(N) of each atom was calculated using the method of Richmond (*39*), and ASA(U) was obtained as described above (*40*, *41*). The results suggest a 1.2 kcal/mol decrease in ΔG_{NU}^{0} in the mutant protein compared with the ΔG_{NU}^{0} of the wild-type, which is in agreement with the experimentally observed difference in ΔG_{NU}^{0} between the two proteins. The results also suggest that the residues at which the difference in the ΔASA between the wild-type and the mutant is large contribute to the change in stability between the two proteins (see Figure 6). Among them, the residues at the mutation sites are responsible for the decrease in the stability of the mutant. This is consistent with the in vivo folding studies of this protein which indicate that the hydrophobicity of Trp64 is important in the stability of human lysozyme, especially when the Cys65−Cys81 or the Cys77−Cys95 disulfide bond is eliminated (*22*).

Structure in the Intermediate and the Transition State of Folding. Information regarding the structure around the mutation sites in the intermediate and the transition state of folding can be inferred from difference free energies and the *m* values of the states obtained from the analysis of kinetic folding measurements (Table 2).

(1) Difference Free Energies. A difference free energy in a state between the mutant and wild-type proteins indicates if the structure around the mutation site is formed in that state (*42*). The difference free energies are defined as follows:

$$\Delta\Delta G_{NU}^{0} = \Delta G_{NU}^{0}(m) - \Delta G_{NU}^{0}(w)$$

$$\Delta\Delta G_{IU}^{0} = \Delta\Delta G_{NU}^{0} - RT \ln[k_{IN}^{0}(m)k_{NI}^{0}(w)/k_{IN}^{0}(w)k_{NI}^{0}(m)] \quad (4)$$

$$\Delta\Delta G_{\ddagger U}^{0} = \Delta\Delta G_{NU}^{0} - RT \ln[k_{NI}^{0}(w)/k_{NI}^{0}(m)]$$

where $\Delta\Delta G_{NU}^{0}$, $\Delta\Delta G_{IU}^{0}$, and $\Delta\Delta G_{\ddagger U}^{0}$, respectively, are the difference free energies of the native, the intermediate, and the transition states relative to the unfolded state, and m and w show the mutant and the wild-type, respectively. If $\Delta\Delta G_{iU}^{0}$ (i = I and ‡) is zero, the structure around the mutation site is not formed in the *i* state, while the larger value of $\Delta\Delta G_{iU}^{0}$ indicates that the structure is partially, or fully, formed in the *i* state around the mutation sites. These values are calculated using the kinetic parameters listed in Table 2, and the Gibbs' free-energy diagrams are constructed as shown in Figure 7. The results show that whereas the $\Delta\Delta G_{NU}^{0}$ is

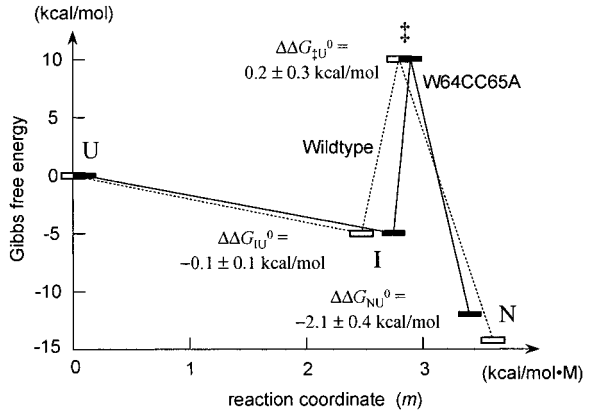

FIGURE 7: The Gibbs' free-energy diagrams of wild-type (dotted lines) and W64CC65A (solid lines) human lysozymes at 0 M GdnHCl drawn using the values given in Table 2. The reaction coordinate is represented by the *m* values.

2.1 kcal/mol, the $\Delta\Delta G_{IU}{}^0$ and $\Delta\Delta G_{\ddagger U}{}^0$ are almost zero. This suggests that the structure around the loop region in the β-domain is not yet locked in place both in the intermediate and the transition state and that the effect of the difference in the disulfide bond location is reflected only in the native state. This is consistent to the present results of the stopped-flow CD and fluorescence measurements which show that the burst-phase intermediates of the wild-type and the mutant proteins have similar secondary structure and similar environment around the tryptophan residues.

(2) *The m* values The m_{ij} value is related to the difference in the solvent-exposed hydrophobic surface between *i* and *j* states (*i*,*j* = U, I, ‡, or N). If the degree of burial of hydrophobic residues is regarded as a measure of the degree of structural organization in each state, the comparison of m_{ij} values determines the position of each state in the reaction coordinate (Figure 7, Table 2). Here, the position of the native (unfolded) state of the mutant on the reaction coordinate is set at the place 0.2 kcal/mol M smaller (0.1 kcal/mol M larger) than the position of the native (unfolded) wild-type protein (see above). Figure 7 suggests that the unfolded, the intermediate, and the transition states of the mutant protein are slightly more organized than the corresponding states of the wild-type protein, while only the native state of the mutant is less organized than the corresponding state of the wild-type. As noted above, the difference in the $m_{NU}{}^{eq}$ between the wild-type and the mutant can be attributed to the difference in the side-chain packing of hydrophobic residues in the 61−80 loop region. Therefore, the present results may suggest that the hydrophobic residues in the 61−80 loop region are not yet buried inside a protein molecule in the intermediate and the transition state of folding.

Folding Mechanism of Human Lysozyme. The above analyses indicate that, in the intermediate and the transition state of folding, the structure around the loop region is not yet formed, suggesting that the structural formation around the 61−80 loop region occurs after the transition state. Hooke et al. (*19*) measured the kinetic refolding of the wild-type human lysozyme using pulsed-hydrogen exchange NMR experiments. The results show that the intermediate formed within a few milliseconds of refolding has stable A-, B-, and 3_{10}-helices in the α-domain and suggest that a hydrophobic cluster and some tertiary interactions are formed in the intermediate. On the other hand, the structure in the β-domain is formed late in folding. These results are consistent with our present results.

Taniyama et al. (*18*) studied the refolding and unfolding kinetics of the mutant human lysozyme C77AC95A, in which the Cys77−Cys95 interdomain disulfide bond is eliminated. The results show that whereas the refolding rate of the mutant is similar to that of the wild-type, the unfolding rate of the mutant is significantly higher than that of the wild-type protein, indicating that the structure around the Cys77−Cys95 disulfide bond, i.e., the interdomain region, is formed after the transition state of the folding. Therefore, our present results with those mentioned above suggest that in the folding of human lysozyme both the formation of the β-domain and docking of the α- and the β-domains take place after the transition state of the folding.

REFERENCES

1. Kim, P. S., and Baldwin, R. L. (1990) *Annu. Rev. Biochem. 59*, 631−660.
2. Baldwin, R. L. (1993) *Curr. Opin. Struct. Biol. 3*, 84−91.
3. Kuwajima, K. (1996) in *Circular Dichroism and the Conformational Analysis of Biomolecules* (Fasman, G. D., Ed.) pp 159−182, Plenum Press, New York.
4. Dyson, H. J., and Wright, P. E. (1996) *Annu. Rev. Phys. Chem. 47*, 369−395.
5. Engelhard, M., and Evans, P. A. (1996) *Folding Des. 1*, R31−R37.
6. Plaxco, K. W., and Dobson, C. M. (1996) *Curr. Opin. Struct. Biol. 6*, 630−636.
7. Eaton, W. A., Muñoz, V., Thompson, P. A., Chan, C. K., and Hofrichter, J. (1997) *Curr. Opin. Struct. Biol. 7*, 10−14.
8. Arai, M., Ikura, T., Semisotnov, G. V., Kihara, H., Amemiya, Y., and Kuwajima, K. (1998) *J. Mol. Biol. 275*, 149−162.
9. Serrano, L., Matouschek, A., and Fersht, A. R. (1992) *J. Mol. Biol. 224*, 805−818.
10. Matouschek, A., Serrano, L., and Fersht, A. R. (1992) *J. Mol. Biol. 224*, 819−835.
11. López-Hernández, E., and Serrano, L. (1996) *Folding Des. 1*, 43−55.
12. Dalby, P. A., Oliveberg, M., and Fersht, A. R. (1998) *J. Mol. Biol. 276*, 625−646.
13. Kuwajima, K. (1989) *Proteins 6*, 87−103.
14. Ptitsyn, O. B. (1995) *Adv. Protein Chem. 47*, 83−229.
15. Arai, M., and Kuwajima, K. (1999) *Adv. Protein Chem.* (in press).
16. Herning, T., Yutani, K., Taniyama, Y., and Kikuchi, M. (1991) *Biochemistry 30*, 9882−9891.
17. Radford, S. E., Dobson, C. M., and Evans, P. A. (1992) *Nature 358*, 302−307.
18. Taniyama, Y., Ogasahara, K., Yutani, K., and Kikuchi, M. (1992) *J. Biol. Chem. 267*, 4619−4624.
19. Hooke, S. D., Radford, S. E., and Dobson, C. M. (1994) *Biochemistry 33*, 5867−5876.
20. Haezebrouck, P., Joniau, M., Van Dael, H., Hooke, S. D., Woodruff, N. D., and Dobson, C. M. (1995) *J. Mol. Biol. 246*, 382−387.
21. Matagne, A., and Dobson, C. M. (1998) *Cell Mol. Life Sci. 54*, 363−371.
22. Kanaya, E., and Kikuchi, M. (1992) *J. Biol. Chem. 267*, 15111−15115.
23. Artymiuk, P. J, and Blake, C. C. (1981) *J. Mol. Biol. 152*, 737−762.
24. Muraki, M., Harata, K., Sugita, N., and Sato, K. (1996) *Biochemistry 35*, 13562−13567.
25. Harata, K., Abe, Y., and Muraki, M. (1998) *Proteins 30*, 232−243.
26. Pace, C. N. (1986) *Methods Enzymol. 131*, 266−280.
27. Kikuchi, M., Yamamoto, Y., Taniyama, Y., Ishimaru, K., Yoshikawa, W., Kaisho, Y., and Ikehara, M. (1988) *Proc. Natl. Acad. Sci. U.S.A. 85*, 9411−9415.

28. Pace, C. N., Vajdos, F., Fee, L., Grimsley, G., and Gray, T. (1995) *Protein Sci. 4*, 2411−2423.
29. Arai, M., and Kuwajima, K. (1996) *Folding Des. 1*, 275−287.
30. Chou, P. Y., and Fasman, G. D. (1974) *Biochemistry 13*, 222−245.
31. Chaffotte, A. F., Guillou, Y., Goldberg, M. E. (1992) *Biochemistry 31*, 9694−9702.
32. Woody, R. W., and Dunker, A. K. (1996) in *Circular Dichroism and the Conformational Analysis of Biomolecules* (Fasman, G. D., Ed.) pp 109−157, Plenum Press, New York.
33. Halper, J. P., Latovitzki, N., Bernstein, H., and Beychok, S. (1971) *Proc. Natl. Acad. Sci U.S.A. 68*, 517−522.
34. Schellman, J. A. (1987) *Annu. Rev. Biophys. Biophys. Chem. 16*, 115−137.
35. Shortle, D. (1995) *Adv. Protein Chem. 46*, 217−247.
36. Baldwin, R. L. (1996) *Folding Des. 1*, R1−R8.
37. Kiefhaber, T. (1995) *Proc. Natl. Acad. Sci. U.S.A. 92*, 9029−9033.
38. López-Hernández, E., Cronet, P., Serrano, L., and Muñoz, V. (1997) *J. Mol. Biol. 266*, 610−620.
39. Richmond, T. J. (1984) *J. Mol. Biol. 178*, 63−89.
40. Oobatake, M., and Ooi, T. (1989) *Bull. Inst. Chem. Res. Kyoto Univ. 66*, 433−455.
41. Oobatake, M., and Ooi, T. (1993) *Prog. Biophys. Mol. Biol. 59*, 237−284.
42. Matouschek, A., Kellis, J. T. Jr., Serrano, L., Bycroft, M., and Fersht, A. R. (1990) *Nature 346*, 440−445.
43. Kraulis, P. J. (1991) *J. Appl. Crystallogr. 24*, 946−950.
44. Sharp, K. A., Nicholls, A., Friedman, R., and Honig, B. (1991) *Biochemistry 30*, 9686−9697.

BI9921945